ELSEVIER

Journal of Power Sources 92 (2001) 168–176

JOURNAL OF POWER SOURCES

www.elsevier.com/locate/jpowsour

Preparation and characterization of gold-codeposited $LiMn_2O_4$ electrodes

Mi-Ra Lim[a], Wan-Il Cho[b], Kwang-Bum Kim[c,*]

[a]*Department of Chemistry, Chonnam National University, 300 Yongbong-Dong, Buk-gu, Kwangju 500-757, South Korea*
[b]*Battery & Fuel Cell Research Center, Korean Institute of Science and Technology, PO Box 131, Cheongryang, Seoul 136-791, South Korea*
[c]*Department of Metallurgical Engineering, Yonsei University, 134 Shinchon-dong, Seodaemun-ku, Seoul 120-749, South Korea*

Received 28 April 2000; accepted 5 June 2000

Abstract

Additive-free, gold-codeposited $LiMn_2O_4$ electrodes are prepared by embedding $LiMn_2O_4$ particles in an electrodeposited coating of metallic gold on platinum-coated quartz crystals for microgravimetric evaluation with an electrochemical quartz crystal microbalance. The chemical and structural characteristics of the electrodes are studied by Raman spectroscopy and X-ray diffraction and the electrochemical properties by cyclic voltammetry. Test cells are assembled with the gold-codeposited electrode as the working electrode, lithium foil as the counter electrode and a reference electrode. A 1.0 M lithium perchlorate ($LiClO_4$), propylene carbonate (PC) solution is used as the electrolyte. Gold-codeposited $LiMn_2O_4$ electrodes prepared at deposition times of 4–8 min have a good adhesion of powder to the substrate. The cyclic voltammograms show little difference in the exchanged charge with cycling. Scanning electron microscopy shows fracture of the $LiMn_2O_4$ powders induced by a dimensional mismatch in the particles after cyclic voltammetric tests at high scan rates.

Keywords: $LiMn_2O_4$; Au-codeposited $LiMn_2O_4$ electrode; Electrochemical quartz crystal microbalance fracture of $LiMn_2O_4$ powders

1. Introduction

Several transition metal oxides have been extensively studied as cathode materials for high energy, rechargeable, lithium batteries. Among them, spinel $LiMn_2O_4$ provides an attractive alternative to commercialized $LiCoO_2$ because it is a low-cost, environmentally acceptable material [1]. Unfortunately, spinel $LiMn_2O_4$ shows severe capacity fading with cycling compared with $LiCoO_2$ [2], and thus significant efforts have been devoted to improve this poor performance.

The capacity loss has been ascribed to several possible factors [3,4], (i) namely: slow dissolution of the $LiMn_2O_4$ electrode into the electrolyte according to the disproportion reaction: $2Mn^{3+} \rightarrow Mn^{4+}+Mn^{2+}$; (ii) transformation of an unstable two-phase structure in the high-voltage region to a more stable single-phase structure via a loss of MnO; (iii) electrochemical reaction of the electrolyte at high voltage. The capacity fading phenomenon is primarily linked to the dissolution of the spinel electrode. Jang et al. [5] quantitatively analyzed the dissolution of Mn from a spinel by using differential pulse polarography. It was reported that the capacity loss originates from solvent molecules which are electrochemically oxidized on the carbon surface (conductive material), and then the as-generated species promote manganese dissolution [5]. Most of the electrochemical studies of $LiMn_2O_4$ have been carried out with a composite electrode which consists of powdered electroactive materials an organic binder such as polyvinylidene fluoride (PVdF) and a conductive additive. Consequently, care has to be taken in evaluating the intrinsic kinetic and electrochemical properties of the active material itself when using a composite electrode because it involves interference derived from other additives. To avoid these complications, various strategies have been introduced to produce an additive-free electrode such as a thin film of electrode material on a substrate by deposition techniques including chemical vapor deposition. The deposition techniques include chemical vapor deposition [6], sputtering [7], electrostatic spray

* Corresponding author. Tel.: +82-2-361-2839; fax: +82-2-312-5375.
E-mail address: kbkim@yonsei.ac.kr (K.-B. Kim).

0378-7753/01/$ – see front matter
PII: S0378-7753(00)00518-8

[8], and reactive electron beam evaporation [9,10]. Uchida and Sato [11] described the preparation of $LiCoO_2$ thin films with submicron thickness on gold substrates using a molten-salt technique and reported that electrochemical responses occurred in a propylene carbonate (PC) solution of 1 M $LiClO_4$ [11].

The electrochemical quartz crystal microbalance (EQCM) has been established as a powerful tool for in situ mass-sensitive detection. The technique is based on the measurement of the resonant frequency change induced by mass change in a film attached to a quartz crystal substrate during electrochemical reaction [12]. The EQCM technique may distinguish the insertion/extraction reactions of Li ions in a $LiMn_2O_4$ electrode from other chemical and electrochemical side reactions related to capacity fading, such as the dissolution of manganese ions and oxidative decomposition of solvent on the electrode surface. For a quartz crystal to oscillate, a very small quantity of active materials (ca. 50 μg for the 5 MHz quartz crystal used in the present study) has to be loaded into the quartz crystal because the ratio of the resonant frequency shift to the original resonant frequency should be less than 0.02 [13–15]. Furthermore, since a quartz crystal undergoes a phase transition at 573°C, the preparation of electrode materials should be performed at temperatures below the value for EQCM-based evaluation. The preparation of thin film electrode materials, however, usually requires treatment at temperatures higher than 573°C. This limits the use of the EQCM technique. Therefore, a low-temperature synthesis has to be developed. Park et al. studied lithium insertion in a V_2O_5 xerogel film by means of EQCM in addition to electrochemical methods [16]. The preparation of $LiMn_2O_4$ films usually requires a high operating temperature of around 800°C, which is well above the temperature at which transition occurs in quartz. Yang et al. [17] investigated the intercalation process of Li ions in a spinel $LiMn_2O_4$ electrode prepared by the sol–gel method by using EQCM in the potential region 2–4 V (Li^+/Li). They suggested that the intercalation process can be divided into at least two stages. This implies a co-intercalation of solvent with Li^+ in the second stage. Nishizawa et al. [18] studied the lithium insertion/extraction reaction in a spinel $LiMn_2O_4$ film electrode prepared at 400°C by electrostatic spray deposition using EQCM in a $LiClO_4$-based electrolyte. It was found that the mass response fitted well to the theoretical values, on the assumption of one electron transfer per equivalent of Li.

As part of a larger study, which seeks to determine the causes of the capacity fading of spinel $LiMn_2O_4$ using EQCM, this investigation reports on the preparation of additive-free, gold-codeposited $LiMn_2O_4$ electrodes on platinum-coated quartz crystals using a very small amount of powdered materials, and discusses their electrochemical properties. The chemical and structural characteristics of the codeposited electrodes are studied by means of Raman spectroscopy and X-ray diffraction, and the morphology is studied by means of scanning electron microscopy.

2. Experimental

An Au-codeposited $LiMn_2O_4$ electrode was prepared on a platinum-coated quartz crystal by embedding a very small amount of $Li_{1+x}Mn_2O_4$ powder (Kerr McGee Chemical LLC products, 2l0grode, X=0.06–0.08) in an electrodeposited coating of metallic gold. Gold is electrochemically inert in an electrolyte solution of 1.0 M lithium perchlorate ($LiClO_4$) in PC [11]. The platinum substrate was placed facing upward a gold plating bath. The bath composition is given in Table 1. $LiMn_2O_4$ powders were added (ca. 40 μg) and maintained in suspension by stirring for a few seconds. The particles were then allowed to deposit on the electrode surface through sedimentation in the stagnant solution. A cathodic current of 4.0 mA was applied and metallic gold was deposited on the platinum substrate. The electroactive surface area of the platinum-coated quartz crystal was 0.39 cm^2, and the bath temperature was maintained at 50°C during the deposition. The amount of charge was varied to control the thickness of the gold layer and the surface morphology of the gold-codeposited $LiMn_2O_4$ electrodes. Scanning electron microscopic (SEM) observations were made in the interfacial region between the $LiMn_2O_4$ powder and the gold-coated substrate. Identification of the molecular structure of the $LiMn_2O_4$ powder and the gold-codeposited $LiMn_2O_4$ was made using microRaman spectroscopy to examine any chemical changes in the powders during the preparation of electrodes. The spectra were obtained with a Jobin Yvon T64000 Raman spectrometer equipped with a charge-coupled device (CCD) detector and a TV monitor to observe sample images. The 50× objective lens of the microscope was used to focus the laser beam on a small selected area of the electrode surface. The Raman excitation source was the 514.5 nm line of a Lexel argon laser excited at 100 mW. The crystallographic structure was analyzed by X-ray diffraction using a 1730 Philips diffractometer with Cu Kα radiation.

The electrochemical behavior of the electrode was studied by means of cyclic voltammetry. The test cell comprised the gold-codeposited working electrode, a lithium foil counter electrode and a reference electrode. The electrolyte was 1.0 M lithium perchlorate ($LiClO_4$) in PC solution. SEM observations of the electrodes were made before and after the cyclic voltammetric tests in order to study any morphological change in the $LiMn_2O_4$ powders. Electrochemical measurements were performed in a glove box filled with dried argon.

Table 1
Composition of gold plating bath

Gold as potassium gold cyanide (g/l)	8–20
Monopotassium phosphate (g/l)	80
Potassium citrate (g/l)	70
pH	6.0–8.0

3. Results and discussion

3.1. Characterization of gold-codeposited $LiMn_2O_4$ electrode

The first part of the experiment was conducted to assess whether electrodeposition had modified the active material ($LiMn_2O_4$) during electrode preparation. $LiMn_2O_4$ powders were characterized before and after embedding by using microRaman spectroscopy and X-ray diffraction. Micro-Raman spectra of the pure $LiMn_2O_4$ powder and the gold-codeposited $LiMn_2O_4$ electrode are shown in Fig. 1. The lithium-excess pure $LiMn_2O_4$ powder shows a band centered at 632 cm^{-1} [19] which can be clearly identified in the spectra of the gold-codeposited $LiMn_2O_4$ electrode. The Raman response of the electrodeposited gold is negligible, as shown in Fig. 1(c). The absence of a Raman shift in Fig. 1(a and b) indicates that the molecular structure of the gold-codeposited $LiMn_2O_4$ electrode does not change during preparation of the electrode.

XRD patterns of the $LiMn_2O_4$ powder and the gold-codeposited $LiMn_2O_4$ electrode are compared in Fig. 2. All of the diffraction peaks of the gold-codeposited $LiMn_2O_4$ are attributable to the spinel structure of $LiMn_2O_4$ with the space group Fd 3 m, in which Li and Mn ions occupy 8a tetrahedral sites and 16d octahedral sites, respectively [20]. A broad peak at a 2θ angle of 38.2° is assigned to the co-diffraction line of gold in Fig. 2(b).[1] The data show that there is no change in the crystallographic structure during preparation of the gold-codeposited electrode.

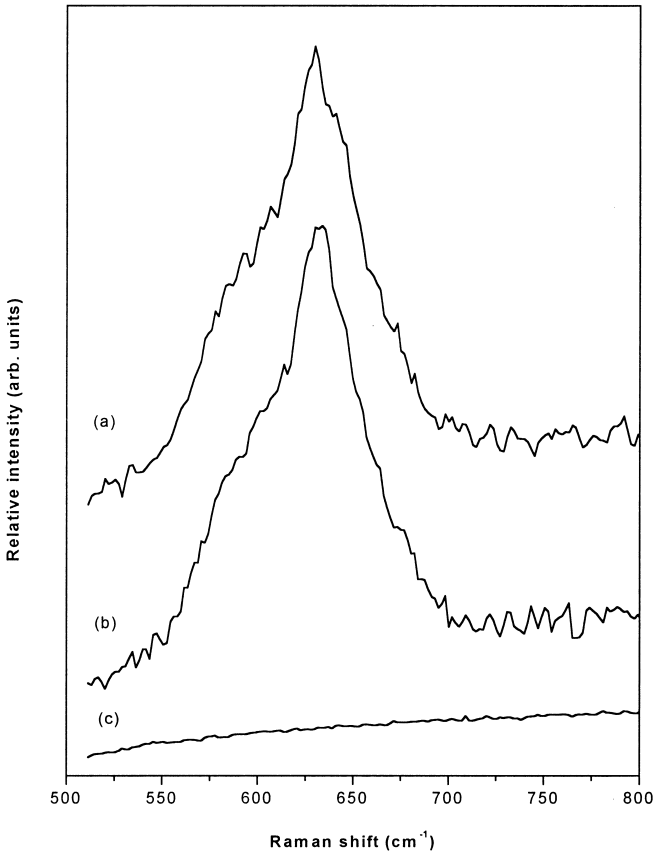

Fig. 1. MicroRaman spectra: (a) $LiMn_2O_4$ powder; (b) gold-codeposited $LiMn_2O_4$ electrode, and (c) electrodeposited gold.

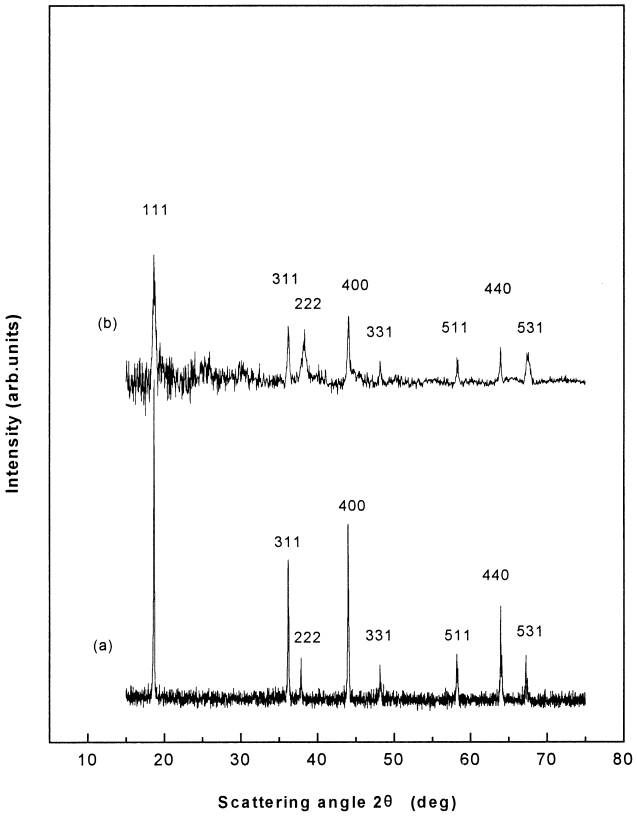

Fig. 2. X-ray diffraction spectra: (a) $LiMn_2O_4$ powder, and (b) gold-codeposited $LiMn_2O_4$ electrode.

Electron micrograhps of the cross-sections of gold-codeposited $LiMn_2O_4$ electrodes prepared with various electroplating durations are presented in Fig. 3. For a deposition time of 2 min, a thin layer of electrodeposited gold is observed on the substrate, but, does not anchor the $LiMn_2O_4$ powder to the substrate (Fig. 3(a)); the powder appears to be loosely attached to the substrate and is barely embedded in the gold layer. At a deposition time of 4 min (Fig. 3(b)), a layer of 1 μm thick gold is formed on the substrate and the $LiMn_2O_4$ powder is anchored to the substrate, but only at the lower ends of the particles. After 8 min of deposition (Fig. 3(c)), gold covers the platinum substrate and the $LiMn_2O_4$ powder is completely anchored to the substrate. Close observation shows that the gold is preferentially electrodeposited at the powder/substrate interface, leading to a good adhesion of the powder to the substrate. For 16 min of deposition (Fig. 3(d)), gold layer envelops the $LiMn_2O_4$ powder, as well as the platinum substrate, and this leaves little $LiMn_2O_4$ for electrochemical reaction.

Top-view electron micrographs of gold-codeposited $LiMn_2O_4$ electrodes prepared with various electroplating

[1] Joint Commission on Powder Diffraction Standards, File 40-784.

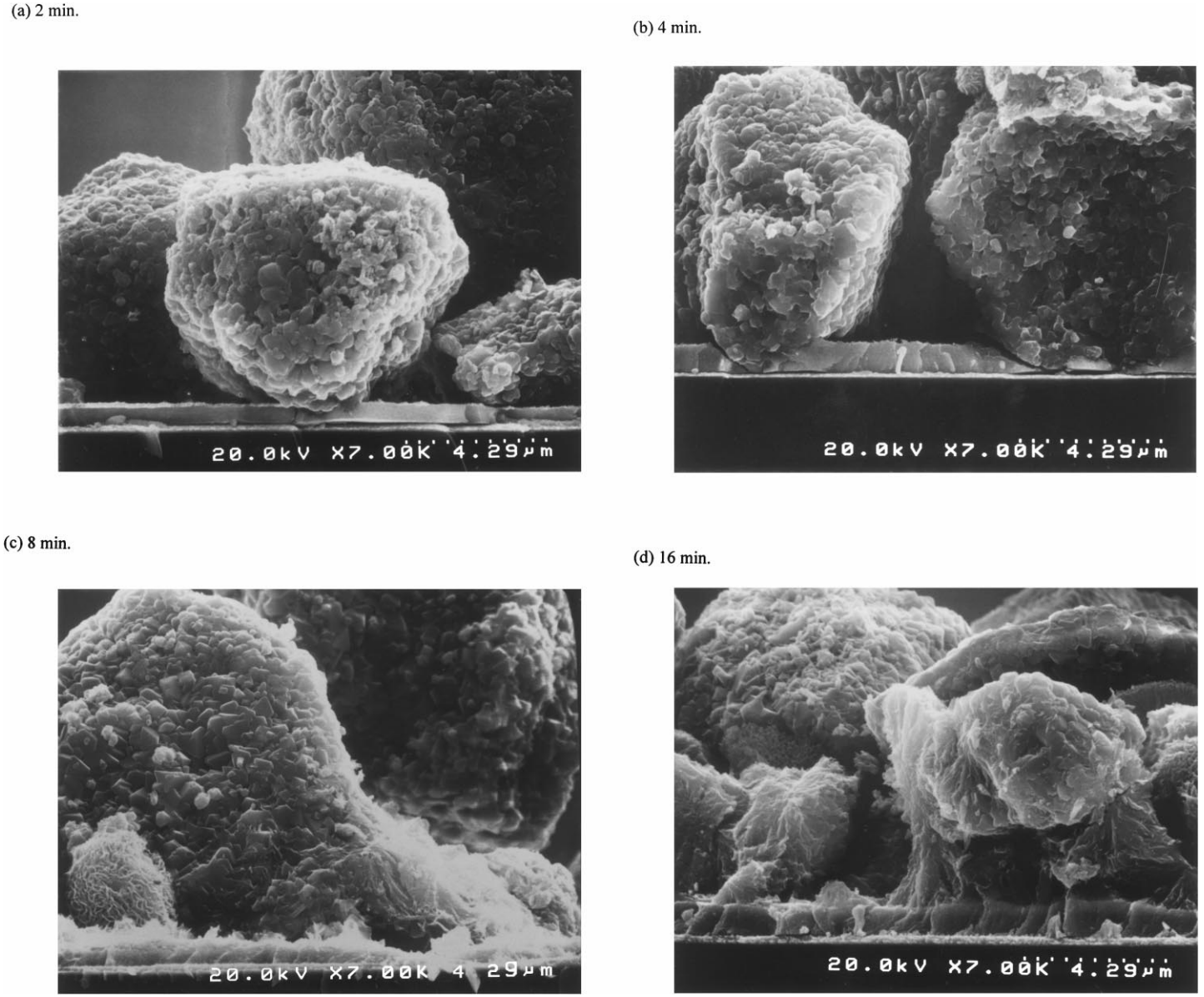

Fig. 3. Electron micrographs of cross-sections of gold-codeposited $LiMn_2O_4$ electrodes prepared with various durations of gold plating.

(a) 2 min.

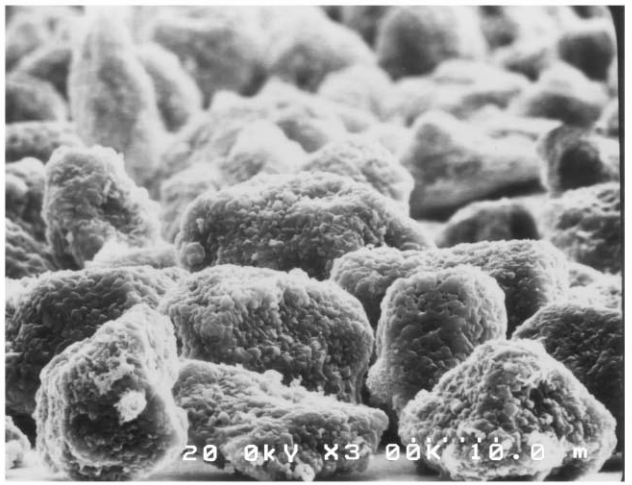

(b) 4 min.

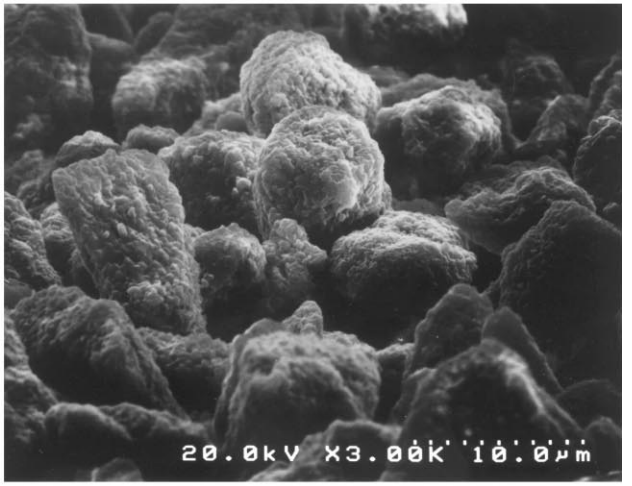

(c) 8 min.

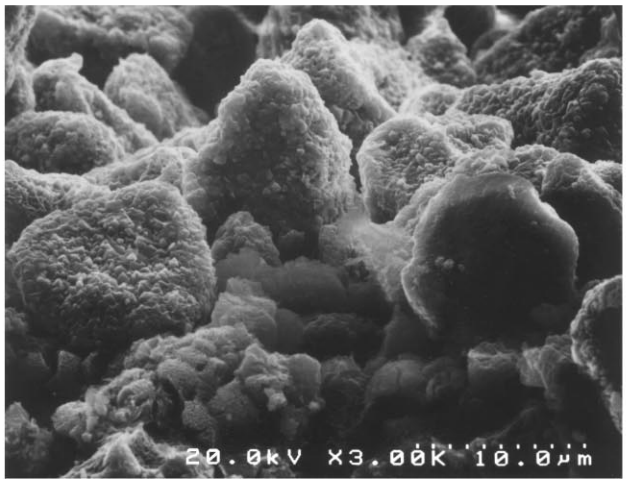

(d) 16 min.

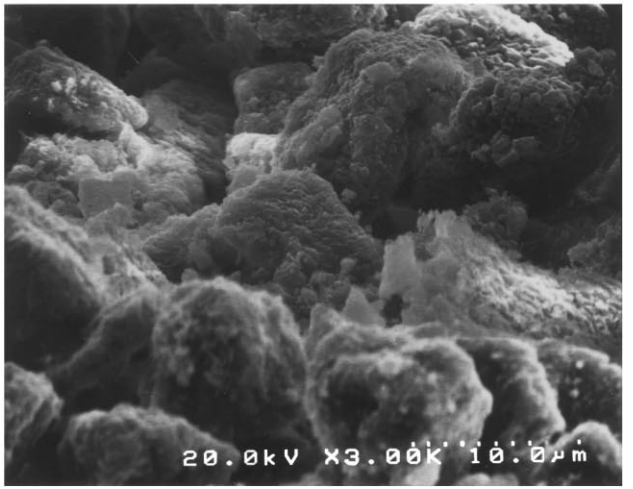

Fig. 4. Electron micrographs (top view) of gold-codeposited $LiMn_2O_4$ electrodes prepared with various durations of gold plating.

durations are presented in Fig. 4. After 2 min of deposition, metallic gold is deposited as patches on the surface and is not in contact with particles. Moreover, the amount of electrodeposited Au is too small to anchor $LiMn_2O_4$ particles to the substrate. At deposition times of 4 and 8 min (Fig. 4(b and c), respectively), the lower ends of the powders and patches of the surface not in contact with the particles are covered with a gold layer, as explained in Fig. 3(b and c). For 16 min of deposition, the platinum substrate is completely covered with a gold layer and $LiMn_2O_4$ powders are buried in the gold layer (Fig. 4(d)). Gold-codeposited $LiMn_2O_4$ electrodes prepared with deposition times of 4 and 8 min allow a good adhesion of the powder to the substrate, and provide active surfaces not covered with a gold layer.

3.2. The electrochemical properties of Au-codeposited $LiMn_2O_4$ electrode

The cyclic voltammogram for electrodeposited gold is given in Fig. 5(a). It may be concluded that the contribution of gold to the voltammetric response of a gold-codeposited $LiMn_2O_4$ electrode is negligible because gold does not produce any electrochemical reaction in this potential range. Cyclic voltammograms of gold-codeposited $LiMn_2O_4$ electrodes at deposition times of 30 s, 1 min, and 2 min are shown in Fig. 5(b–d), respectively. An important feature of the voltammograms is the decrease in the exchanged charge on cycling without a shift in the peak potentials. This means that capacity fading on cycling is due to the gradual isolation of the loosely attached particles from the substrate caused by poor adhesion. Cyclic voltammograms for electrodes at deposition times of 4, and 8 and 16 min, are presented in Fig. 5(e–g), respectively. There is virtually no decrease in the exchanged charge with cycling. This indicates that $LiMn_2O_4$ particles are completely embedded in the gold layer with good adhesion to the substrate. Well-defined, reversible peaks for Li extraction/intercalation in the spinel $LiMn_2O_4$ lattice are found for gold-codeposited $LiMn_2O_4$ electrodes around 4.0 and 4.1 versus Li/Li^+. This is in good agreement with the results of Nishizawa et al. [21] and Totir et al. [22]. Two pairs of redox peaks in the 4 V region correspond to Li ion extraction/insertion in tetrahedral sites [23]. Other researchers have reported that the low-voltage region is for Li ion insertion/extraction in the one-phase structure, and that the high-voltage region is for (de)intercalation of Li between $LiMn_2O_4$ and λ-MnO_2 [3]. Another feature of the cyclic voltammograms in Fig. 5(e–g) is the difference in peak currents at various gold electroplating duration. The peak currents gradually decrease with increase in the deposition time from 4 to 16 min, e.g. the peak currents in Fig. 5(g) are half of those observed in Fig. 5(e). This means that $LiMn_2O_4$ powders are partly buried in the gold layer, and these buried particles are inactive during electrochemical reaction. This is consistent with the SEM observations presented in Figs. 3 and 4. The cyclic voltammogram of a gold-codeposited $LiMn_2O_4$ electrode at a deposition time of 32 min is shown in Fig. 5(h). It can be surmised that most of the $LiMn_2O_4$ particles are covered with gold because the characteristic current peaks of $LiMn_2O_4$ are not observed.

The scan rate dependence of the cyclic voltammograms is illustrated in Fig. 6. The voltammograms were obtained during the 4–7th cycles of a gold-codeposited $LiMn_2O_4$ electrode at a deposition time of 4 min, between 3.6 and 4.3 V versus Li/Li^+. On increasing the scan rate, the splitting of the peaks becomes obscure, and the potentials of the anodic and cathodic peaks shift to more positive and more negative potentials, respectively. This behavior can be ascribed to the increased *iR* drop due to the electrode resistance [11]. The charge passed during the lithium extraction process is calculated to be between 3.6 and 4.3 V versus Li/Li^+. The amount of charge passed during positive-going potential scans is plotted in Fig. 7 as function of the reciprocal of the scan rates. At scan rates higher than $1\ mV\ s^{-1}$, the amount of charge decreases rapidly. This indicates that the scan rates are too fast to complete the oxidation of the entire gold-codeposited $LiMn_2O_4$ electrode. The electrode appears to respond fully to the extraction of Li ions at rates lower than $0.5\ mV\ s^{-1}$, where the amount of charge is almost constant. The second peak current versus $\upsilon^{1/2}$ for both positive-going and negative-going scans is given in Fig. 8. The plots are found to be linear for both scans, and the mean chemical diffusion coefficient of Li^+ in the lattice over the extraction/insertion process yields values of the order $10^{-11}\ cm^2\ s^{-1}$; this is in good agreement with the value reported by Johnson et al. [24].

Electrochemical charge and discharge is usually accompanied by a change in the lattice dimensions of a solid matrix. Lattice dimensions are usually a function of the degree of reaction, so that stress is induced by strain due to a dimensional mismatch between regions with different degrees of reaction [25]. There have been a few reports on the mechanical fracture of electrode materials during electrochemical charging and discharging. Ohzuku et al. [26] performed charging and discharging of Li/MnO_2 cells in the voltage range of 2.0–4.0 V, while employing acoustic emission to monitor the particle fracture of manganese dioxide. They reported that acoustic events concentrated at the end of discharge, while no event was observed during the charge. This indicates that a particle fracture takes place during the insertion of lithium ions in a solid matrix. They observed that a higher current causes a higher rate of acoustic events. Waki et al. [27] reported on particle splitting during the Li ion extraction/insertion process in a single particles of $LiCoO_2$ and $LiNiO_2$ using an optical microscope equipped with a CCD camera and a video recorder [27]. In these cyclic voltammertric tests, the positive potential limit was intentionally expanded up to 5.2 V in an organic solution containing $LiClO_4$, and they observed that most particles are split into several pieces at about 4.5 V in the first scanning of $LiNiO_2$, but not for $LiCoO_2$. Recently, Shao-Horn et al. [28] detected small nanoscale crystallites which

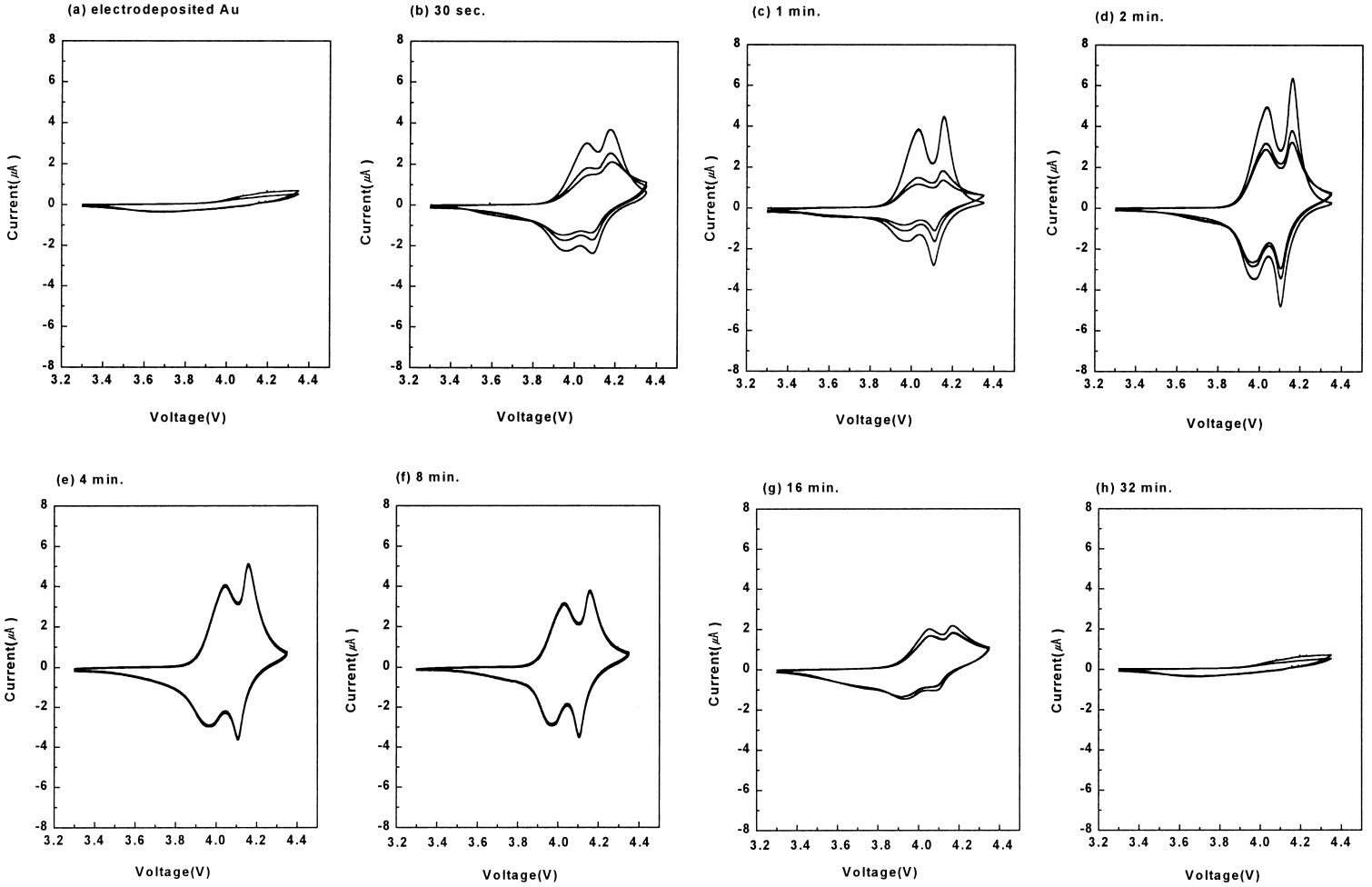

Fig. 5. Cyclic voltammograms for (a) electrodeposited gold and (b)–(h) gold-codeposited $LiMn_2O_4$ electrodes prepared with various durations of gold plating. Sweep rate 0.1 mV s^{-1}, potential range 3.3–4.35 V.

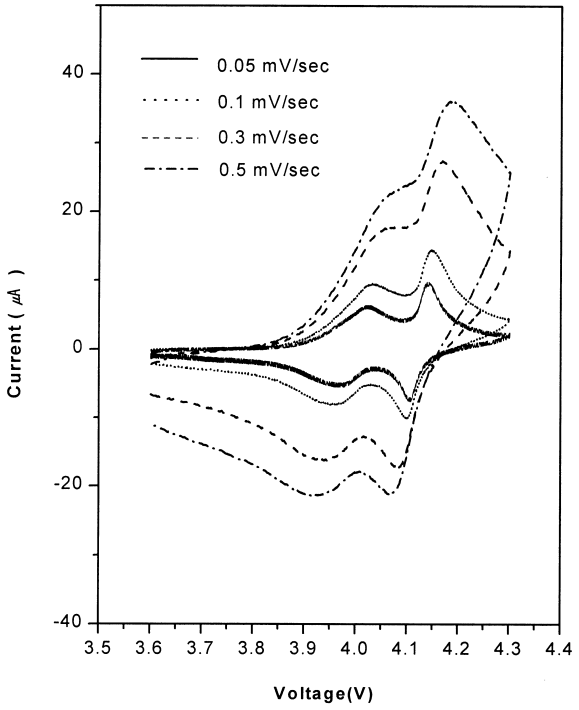

Fig. 6. Scan rate dependence of cyclic voltammograms for a Au-codeposited $LiMn_2O_4$ electrode in $LiClo_4$/PC.

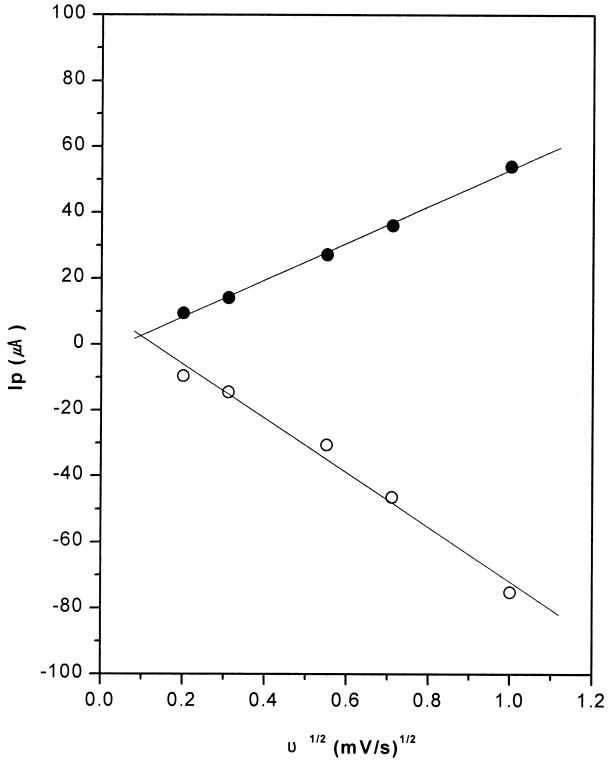

Fig. 8. Plot of peak current vs. $\upsilon^{1/2}$ for (●) positive-going and (○) negative-going scans.

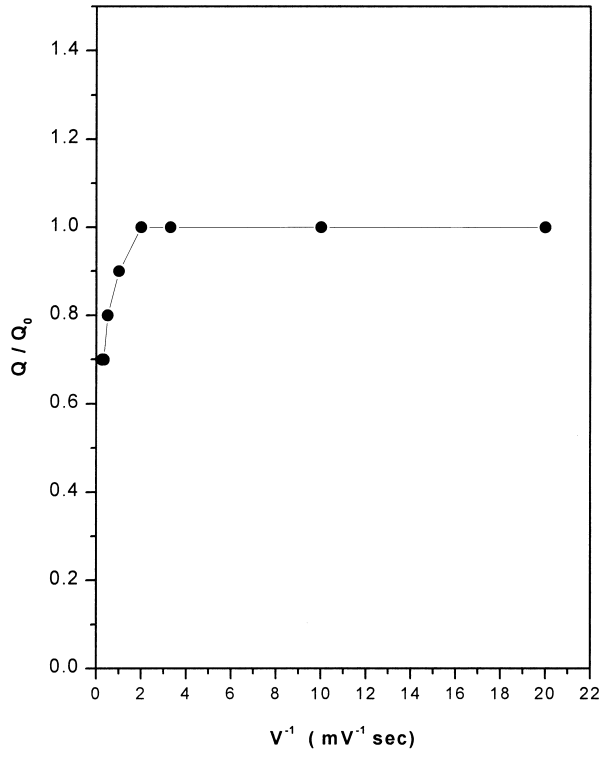

Fig. 7. Plot of charge passed during positive-going potential scans against the reciprocal of scan rate. (Q_0 is the amount of charge at a scan rate of 0.05 mV s^{-1}).

appeared to have separated from the larger crystallites in the particles during cycling between 3.3 and 2.2 V in Li/$Li_xMn_2O_4$ coin cells by using transmission electron microscopy. They found structural fatigue on the surface of discharged $Li_xMn_2O_4$ spinel electrodes cycled at voltages above 3 V and proposed that the presence of $Li_2Mn_2O_4$ on the particle surface may contribute to some of the capacity fading observed during the cycling of a Li/$LiMn_2O_4$ cell.

The surface of a discharged gold-codeposited $LiMn_2O_4$ electrode prepared with a deposition time of 4 min was examined after electrochemical experiments by SEM, and is shown in Fig. 9. The cell of the Li/Au-codeposited $LiMn_2O_4$ was cycled twice between 3.5 and 4.35 V versus Li/Li^+ at a scan rate of 4 mV s^{-1}. An evident disruption in the $LiMn_2O_4$ particles (diameter 20 μm) is observed in Fig. 9. This phenomenon was not found, however, at a scan rate of 0.1 mV s^{-1} for the Au-codeposited $LiMn_2O_4$ electrode, even after 50 cycles. The insertion/extraction reactions of Li ions cause internal stress at interfaces between reacted and unreacted regions in a particle, and may thereby lead to particle fracture to release stress. This is because the lattice dimension in a reacted region where the solid matrix accommodates Li ions (and electrons) is usually different from that in the unreacted region at the unit cell level [25]. Particle fracture eventually leads to isolation of $LiMn_2O_4$ fragments from the electrode that, in turn, may cause a catastrophic failure due to electrical shorts, as well as capacity fading of the battery.

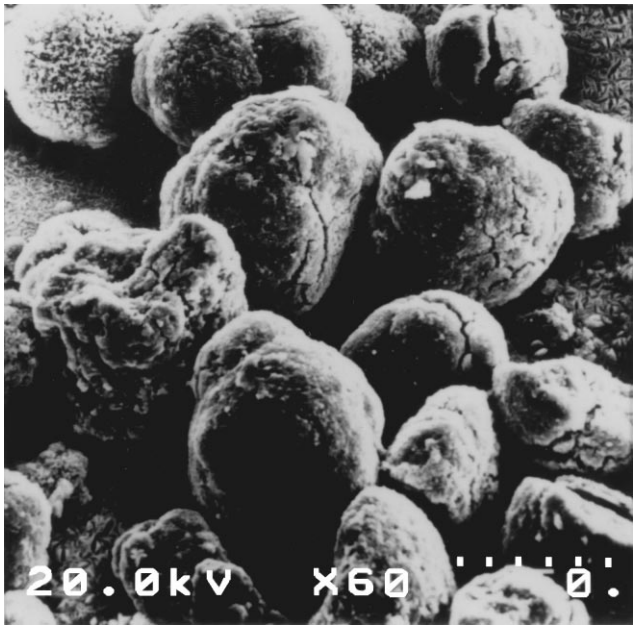

Fig. 9. Electron micrograph of gold-codeposited $LiMn_2O_4$ electrode after cyclic voltammetric tests at a scan rate of 4 mV s^{-1}.

Gold-codeposited $LiMn_2O_4$ electrodes are being used for EQCM evaluation and EQCM data for the Li insertion/extraction reaction in $LiMn_2O_4$ will be reported elsewhere.

4. Conclusions

Gold-codeposited $LiMn_2O_4$ are prepared using a very small amount of the powdered materials for evaluation of their physical and electrochemical properties. MicroRaman spectroscopy and XRD results reveal that the molecular structure of a gold-codeposited $LiMn_2O_4$ electrode do not change during the preparation of the electrode via Au codeposition. Gold-codeposited $LiMn_2O_4$ electrodes prepared with a deposition time of 4–8 min allow a good adhesion of powder to the substrate, The resulting cyclic voltammograms reveal little decrease of the exchanged charge with cycling. SEM observations detail the fracture of $LiMn_2O_4$ powders induced by a dimensional mismatch in a particle after cyclic voltammetric tests at high scan rates.

Acknowledgement

This work was supported by Korean Institute of Science and Technology (KIST) under contract OOHV-051.

References

[1] U. Von Sacken, in: Proceedings of the 15th International Seminar and Exhibit on Primary and Secondary Batteries, Fort Lauderdale, FL, USA, 2–5 March 1998.
[2] Y. Kobayashi, N. Kihira, K. Takei, H. Miyashiro, K. Kumai, N. Terada, P. Ishikawa, J. Power Sources 81/82 (1999) 463.
[3] Y. Xia, M. Zhou, M. Yoshio, J. Electrochem. Soc. 144 (1997) 2593.
[4] R.J. Gummow, A. de Kock, M.M. Thackeray, Solid State Ionics 69 (1994) 59.
[5] D.H. Jang, J.Y. Shin, S.M. Oh, J. Electrochem. Soc. 143 (1996) 2204.
[6] P. Fragnaud, R. Nagarajan, D.M. Schleich, D. Vujic, J. Power Sources 54 (1995) 362.
[7] K.H. Hwang, S.H. Lee, S.K. Joo, J. Electrochem. Soc. 141 (1994) 3296.
[8] C. Chen, E.M. Kelder, J. Schoonman, J. Electrochem. Soc. 144 (1997) L289.
[9] F.K. Shokoohi, J.M. Tarascon, B.J. Wilkens, Appl. Phys. Lett. 59 (1991) 1260.
[10] J.B. Bates, D. Lubben, N.J. Dudney, F.X. Hart, J. Electrochem. Soc. 142 (1995) L149.
[11] I. Uchida, H. Sato, J. Electrochem. Soc. 142 (1995) L139.
[12] D.A. Buttry, M.D. Ward, Chem. Rev. 92 (1992) 1355.
[13] G. Sauerbrey, Phys. Verhandl. 8 (1957) 113.
[14] G. Sauerbrey, Z. Phys. 155 (1959) 206.
[15] P. Lostis, Rev. Opt. (1959) 38.
[16] H.K. Park, W.H. Smyrl, M.D. Ward, J. Electrochem. Soc. 142 (1995) 1068.
[17] Y. Yang, D. Shu, H. Yu, X. Xia, Z.G. Lin, J. Power Sources 65 (1997) 227.
[18] M. Nishizawa, T. Uchiyama, T. Itoh, T. Abe, I. Uchida, Langmuir 15 (1999) 4959.
[19] W. Huang, R. Frech, J. Power Sources 81/82 (1999) 616.
[20] D. Zhang, B.N. Popov, R.E. White, J. Power Sources 76 (1998) 81.
[21] M. Nishizawa, T. Uchiyama, K. Dokko, K. Yamada, T. Matsue, I. Uchida, Bull. Chem. Soc. Jpn. 71 (1998) 2011.
[22] D.A. Totir, B.D. Cahan, D.A. Scherson, Electrochim. Acta 45 (1999) 161.
[23] Y. Xia, M. Yoshio, J. Electrochem. Soc. 143 (1996) 825.
[24] B.J. Johnson, D.H. Doughty, J.A. Voigt, T.J. Boyle, J. Power Sources 68 (1997) 634.
[25] T. Ohzuku, A. Veda, Solid State Ionics 69 (1994) 201.
[26] T. Ohzuku, H. Tomura, K. Sawai, J. Electrochem. Soc. 144 (10) (1997) 3496.
[27] S. Waki, K. Dokko, T. Matsue, I. Uchida, Denki Kagaku 65 (11) (1997) 954.
[28] Y. Shao-Horn, S.A. Hackney, A.J. Kahalan, K.D. Kepler, E. Shinner, J.T. Vaughey, M.M. Thackeray, J. Power Sources 81/82 (1999) 496.